Russian Geology and Geophysics © 2020, V.S. Sobolev IGM, Siberian Branch of the RAS
Vol. 61, No. 12, pp. 1345–1353, 2020 *DOI:10.15372/RGG2019146* *Geologiya i Geofizika*

Phase Relations of Iron Carbides Fe_2C, Fe_3C, and Fe_7C_3 at the Earth's Core Pressures and Temperatures

N.E. Sagatov[a,b,✉], P.N. Gavryushkin[a,b], I.V. Medrish[c,d], T.M. Inerbaev[a,e], K.D. Litasov[f,g]

[a]*V.S. Sobolev Institute of Geology and Mineralogy, Siberian Branch of the Russian Academy of Sciences, pr. Akademika Koptyuga 3, Novosibirsk, 630090, Russia*

[b]*Novosibirsk State University, ul. Pirogova 1, Novosibirsk, 630090, Russia*

[c]*International Research Center for Theoretical Materials Science, Samara State Technical University, ul. Molodogvardeiskaya 244, Samara, 443100, Russia*

[d]*Samara Center for Theoretical Materials Science, Samara National Research University, ul. Akademika Pavlova 1, Samara, 443011, Russia*

[e]*L.N. Gumilyov Eurasian National University, ul. Satbaeva 2, Astana, 010008, Kazakhstan*

[f]*Vereshchagin Institute for High Pressure Physics, Russian Academy of Sciences, Kaluzhskoe sh. 14, Troitsk, Moscow, 108840, Russia*

[g]*Fersman Mineralogical Museum, Russian Academy of Sciences, Leninskii pr. 18/2, Moscow, 119071, Russia*

Received 21 February 2019; received in revised form 23 April 2019; accepted 28 August 2019

Abstract—Based on first-principle calculations in the framework of the density functional theory and structure prediction algorithms, we have determined iron carbide phases stable at the Earth's core pressures and temperatures. It is shown that Fe_7C_3 is unstable and decomposes into the mixture Fe_2C + Fe_3C over the entire range of pressures and temperatures specific to the Earth's inner core. Subsequent decomposition of Fe_3C into the mixture Fe + Fe_2C is unfavorable. We also predict a new low-temperature modification Fe_3C-*C*2/*m*-II dynamically and thermodynamically stable over the pressure range 290–305 GPa.

Keywords: iron carbides; USPEX; AIRSS; crystal structure prediction; quasi-harmonic approximation

INTRODUCTION

The Fe–C system is crucial in studies of the composition of the Earth's inner core (Wood, 1993; Wood et al., 2013). This is because carbon is the fourth abundant element in the Solar System. Its content in carbonaceous chondrites (CI) reaches 3.2 wt.%. Numerous intermediate compositions of the Fe–C system (Fe_3C, Fe_3C_2, Fe_5C_2, Fe_7C_3, and Fe_2C) (Chabot et al., 2008; Lord et al., 2009; Nakajima et al., 2009; Weerasinghe et al., 2011; Bazhanova et al., 2012) were considered as a possible carbon-containing phase in the core.

The Fe–C phase diagram was thoroughly studied at 0–15 GPa. At these pressures two main carbides are distinguished in the system: Fe_3C and Fe_7C_3 (Chabot et al., 2008; Nakajima et al., 2009). Nevertheless, it was shown in theory that iron carbide Fe_7C_3 is less energetically favorable at inner core pressures (>330 GPa) than a mechanical mixture of Fe_2C and Fe_3C at 0 K (Weerasinghe et al., 2011). No calculations were made which would take into account thermal vibrations of atoms and characterize the high-temperature stability of Fe_7C_3, Fe_3C, and Fe_2C.

Under standard conditions Fe_3C crystallizes as cementite (*Pnma*), the stability of which was demonstrated experimentally up to 250 GPa (Takahashi et al., 2012). A random search revealed a new structure, with the *Cmcm* symmetry, which was more favorable than cementite at >326 GPa (Weerasinghe et al., 2011). In the work on structure prediction (Bazhanova et al., 2012), evolutionary algorithms were used to find two other structures with the *I*-4 and *C*2/*m* symmetry which were even more energetically favorable.

The carbide Fe_2C forms in quenched steels as ε-carbide with the $P6_3/mmc$ symmetry (Jack, 1951). In quenched martensite, Fe_2C occurs as another polymorphic form, η-Fe_2C, which is isostructural with Co_2N and Co_2C (Hirotsu and Nagakura, 1972). Ab initio calculations showed that the η-Fe_2C phase is more energetically favorable than ε-Fe_2C at ambient pressure (Lv et al., 2008). A new structure, Fe_2C-*Pnma*, was detected at 150 GPa by random search with an AIRSS program complex (Weerasinghe et al., 2011). Another Fe_2C-*Pnma* structure was found by the evolution-

✉Corresponding author.
E-mail address: sagatinho23@gmail.com (N.E. Sagatov)

ary method using the USPEX code (Bazhanova et al., 2012). Presently, both phases are denoted as Fe_2C-*Pnma*, and no structural comparison between them has been made. Hereinafter, the phase predicted using the AIRSS algorithm (Weerasinghe et al., 2011) is called Fe_2C-*Pnma*-I, and the phase predicted using the USPEX algorithm (Bazhanova et al., 2012) is Fe_2C-*Pnma*-II. Ab initio calculations indicate that the transition from η-Fe_2C to Fe_2C-*Pnma*-II at 0 K takes place at a pressure of about 28 GPa (Litasov et al., 2015). This result, as the decomposition of Fe_7C_3, refers to a temperature of 0 K.

We performed a detailed search for new Fe_2C and Fe_3C structures and analyzed the influence of temperature within quasi-harmonic approximation on the stability of known and new phases of Fe_7C_3, Fe_3C, and Fe_2C.

METHODS

The structure search was performed with the USPEX (Glass et al., 2006; Oganov and Glass, 2006; Oganov et al., 2006; Lyakhov et al., 2010, 2013) and AIRSS (Pickard and Needs, 2006, 2011) program complexes, using fundamentally different approaches. Both methods proved effective in predicting the crystal structures of a wide range of compounds (Weerasinghe et al., 2015; Bazhanova et al., 2017; Gavryushkin et al., 2017, 2018; Smith et al., 2018), including carbides (Weerasinghe et al., 2011; Bazhanova et al., 2012) and related iron nitrides (Gavryushkin et al., 2018).

Calculation of electronic structure was carried out under the density functional theory (DFT) by the pseudopotential method with the VASP 5.3 program complex (Kresse and Furthmüller, 1996; Kresse and Joubert, 1999). Exchange-correlated interaction was taken into account in the Perdew–Burke–Ernzerhof (PBE) generalized gradient approximation (Perdew et al., 1996). The choice of pseudopotential was carried out based on a test with reproducing the experimental (Sata et al., 2010) and theoretical (Bazhanova et al., 2012; Litasov et al., 2015) pressure dependence of the volume of the studied phases (Fig. 1). According to the latest theoretical (Vočadlo et al., 2002; Mookherjee, 2011; Litasov et al., 2015) and experimental studies (Ono and Mibe, 2010; Chen et al., 2012), the magnetic moment for Fe_3C disappears at 40–65 GPa, and the magnetic moment for Fe_2C disappears at 100 GPa. Therefore, calculations at higher pressures were made without regard to spin polarization.

Structure prediction was carried out for the Fe_2C and Fe_3C compositions at 100, 200, 300, and 400 GPa for two, three, and four formula units. The number of first-generation structures in the calculations by the USPEX algorithm was equal to 50. After their optimization, 60% structures with the lowest enthalpy were chosen. They were used for a new generation in the following percentage: 35% were generated by inheritance; 20%, by atomic mutations; 10%, by permutation of lattice parameters; and 35%, by the random method. In the calculations by the AIRSS algorithm, 1000–1200 structures were generated by the random method and optimized, with the choice of the most energetically favorable ones. The optimization in all the calculations was carried out under the DFT by the conjugate gradient algorithm. The optimization parameters were as follows: plane-wave basis cutoff energy, 450 eV; Monkhorst–Pack grid of k-points (Monkhorst and Pack, 1976) with a density of 0.5 $Å^{-1}$; electron smearing by the Methfessel–Paxton scheme (Methfessel and Paxton, 1989); parameter $\sigma = 0.05$ eV. The atomic positions of the most promising of the predicted structures were optimized with higher accuracy: cutoff energy, 600 eV; density of k-points, 0.2 $Å^{-1}$; parameter $\sigma = 0.01$ eV.

To analyze the temperature effect, we used the method of lattice dynamics in the quasi-harmonic approximation. For this purpose, the frequencies of lattice vibrations were calculated. The cutoff energy in this case was equal to 800 eV.

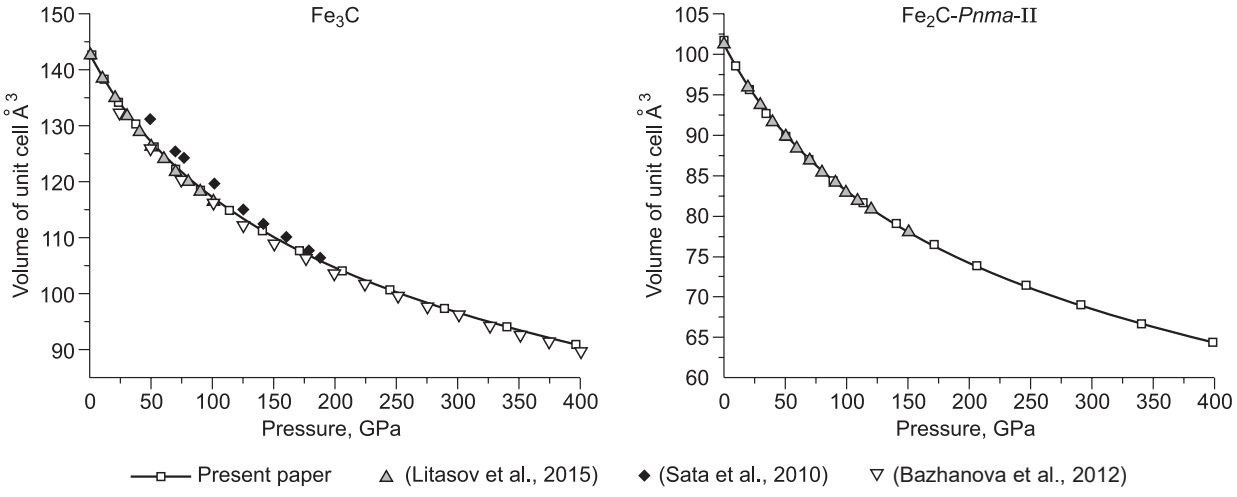

Fig. 1. Relationship between the theoretical and experimental pressure dependences of the volume of the unit cell for cementite (Fe_3C) and Fe_2C-*Pnma*-II at 300 K.

In calculations by the lattice dynamics method, the Helmholtz free energy of a system of volume V at temperature T has the form

$$F(V,T) = F_0(V) + F_{vib}(V,T) + F_{el}(V,T), \quad (1)$$

where $F_0(V)$ is the static-lattice energy; $F_{vib}(V, T)$, the contribution of vibrations to free energy; $F_{el}(V, T)$, electronic contribution to free energy.

The vibrational contribution in the quasi-harmonic approximation can be written as

$$F_{vib}(V,T) = \sum_{q,i}\left[\frac{1}{2}\hbar\omega_{q,i} + k_B T \ln\left(1 - e^{-\frac{\omega_{q,i}}{k_B T}}\right)\right], \quad (2)$$

where $\hbar$ is the Planck constant; k_B, the Boltzmann constant; $\omega_{q,i}$, frequency of vibrations of the i-th mode at q-point; T, temperature.

For dielectric materials, the electronic contribution to free energy is negligible. For metals, this contribution should be taken into account, because it becomes significant as temperature increases. Thus, the electronic free energy has the form

$$F_e(V,T) = E_e(V,T) + TS_e(V,T). \quad (3)$$

Here, $E_e(V, T)$ is the electronic internal energy; $S_e(V, T)$, electron entropy.

For electrons, E_e and S_e are expressible in terms of the Fermi–Dirac distribution function and the electronic density of states:

$$E_e(V,T) = \int_0^\infty n(\varepsilon,V) f(\varepsilon)\varepsilon d\varepsilon + \int_0^{\varepsilon_F} n(\varepsilon,V)\varepsilon d\varepsilon, \quad (4)$$

$$S_e(V,T) = \int_0^\infty n(\varepsilon,V)\left[f\ln f + (1-f)\ln(1-f)\right]d\varepsilon, \quad (5)$$

where ε is the Kohn–Sham orbital energy; ε_F, Fermi level energy; $n(\varepsilon, V)$, electronic density of states; $f(\varepsilon)$, Fermi–Dirac distribution function.

Note that $n(\varepsilon,V) = \frac{1}{N_k}\sum_{k,i}\delta\left(\varepsilon(V) - \varepsilon_{k,i}(V)\right)$, where k is the wave vector and i is the energy eigenvalue index, does not depend on temperature. The temperature dependence in this case is manifested only through the Fermi–Dirac function.

Having calculated the volume dependence of the Helmholtz free energy at the given temperature, we can write down pressure as $P = -(\partial F/\partial V)_T$. So, knowing the volume and temperature dependences of pressure, we can calculate the Gibbs free energy: $G = F + PV$.

Phonon dispersion curves were calculated using the PHONOPY program code (Togo and Tanaka, 2015), and structures were visualized using the VESTA program (Momma and Izumi, 2011). The symmetry and pseudosymmetry of the predicted structures were analyzed with the FindSym (Stokes and Hatch, 2005) and Pseudo programs (Kroumova et al., 2001). The choice of compounds and topological analysis were performed with the ToposPro structural and topological software package (Blatov, 2006; Blatov et al., 2014). The adjacency matrix was calculated by the solid angle method, and the structure topology was determined in the full representation (with regard to all the atoms of the structure). The search for topological correlations was performed in the ICSD_2018_1 structural database of the TORIS Client service (topospro.com).

RESULTS AND DISCUSSION

Iron carbide Fe_3C. The results of prediction of Fe_3C structures at 100–400 GPa are presented in Table 1. The search for low-enthalpy structures detected the Fe_3C structures predicted in the earlier works (Weerasinghe et al., 2011; Bazhanova et al., 2012): cementite, *Cmcm*, and *I*-4. Also, both methods made it possible to find a new structure, Fe_3C-*C*2/*m*. It differs from the structure with the same symmetry (*C*2/*m*) detected in (Bazhanova et al., 2012). Hereinafter, the structure from (Bazhanova et al., 2012) will be denoted as *C*2/*m*-I, and that from the present study will be denoted as *C*2/*m*-II. The structural data on the *C*2/*m*-II modifications are given in Table 2.

The *C*2/*m*-II structure is a monoclinic analog of the *Cmcm* structure, predicted in (Weerasinghe et al., 2011). In the *C*2/*m*-II structure, the carbon coordination number is equal to 9, and the coordination polyhedron is a tricapped trigonal prism. At 300 GPa, the difference between the enthalpies of *C*2/*m*-II and *Cmcm* is ~18 meV/f.u., and it remains constant up to 400 GPa.

Table 1. Predicted structures with the lowest relative enthalpy at different pressures compared to the earlier studies

P, GPa	USPEX		AIRSS		(Bazhanova et al., 2012)		(Weerasinghe et al., 2011)	
	Space group	*Z*	Space group	*Z*	Space group	*Z*	Space group	*Z*
100	*Pnma*	4	*Pnma*	4	*Pnma*	4	*Pnma*	4
200	*Pnma*	4	*Pnma*	4	*Pnma*	4	*Pnma*	4
300	*C2/m*	4	*C2/m*	4	*Pnma*	4	*Pnma*	4
400	*C2/m*	4	*I*-4	8	*I*-4, *C2/m*	8.8	*Cmcm*	4

Note. *Z*, number of formula units in the unit cell.

Table 2. Structural data on the predicted Fe_3C phase

Phase	Pressure, GPa	Space group	Lattice parameters (Å, deg)			Atom coordinates			
						Atom	*x*	*y*	*z*
*C*2/*m*-II	300	*C*2/*m* (#12)	*a* = 7.360	*b* = 2.232	*c* = 5.827	Fe1	0.3718	0.00000	0.55424
						Fe2	0.36303	0.00000	–0.06767
			α = 90.00	β = 93.075	γ = 90.00	Fe3	0.06651	0.0000	0.75963
						C	0.75355	0.00000	0.73381

The *C*2/*m*-II phase narrows down the stability field of cementite, which remains stable up to 302 GPa. Above this pressure, it transforms into the *C*2/*m*-II phase, which is stable up to ~400 GPa (Fig. 2*a*). Above this pressure, the *I*-4 and *C*2/*m*-I phases become more energetically favorable than *C*2/*m*-II. The contribution of zero vibrations to enthalpy has a considerable influence on the pressure of phase transitions. As a result, the *I*-4 phase becomes stable over the pressure range of the Earth's inner core; cementite turns into the *C*2/*m*-II phase at 291 GPa, and *C*2/*m*-II turns into *I*-4 at 305 GPa (Fig. 2*b*). Phonon dispersion curves confirm the dynamic stability of cementite and the predicted *I*-4, *C*2/*m*-I, and *C*2/*m*-II phases at the Earth's core pressures (Fig. 3).

The *P–T* diagram plotted based on the quasi-harmonic approximation (Fig. 4) shows that the wide stability field of the *I*-4 phase covers the entire pressure and temperature range of the Earth's inner core. The predicted *C*2/*m*-II phase is a low-temperature phase. The upper limit of its stability does not exceed 300 K. Above this temperature, the *C*2/*m*-II phase transforms into cementite and Fe_3C-*I*-4. The *C*2/*m*-I phase has no stability field in the considered pressure interval up to 400 GPa.

The performed analysis of the pseudosymmetry of the Fe_3C-*I*-4 structure showed that symmetry increases to *I*-42*m* in the case of atomic displacement for distances of no more than 0.4 Å. However, the more symmetric *I*-42*m* modification turns out to be less energetically favorable in the entire temperature interval.

Iron carbides Fe_2C. As it is stated above, two Fe_2C structures with the *Pnma* symmetry were predicted: *Pnma*-I and *Pnma*-II. According to our topological analysis, these are two different structures characterized by different coordination polyhedra and their relative positions. In the *Pnma*-I structure, the carbon atoms are surrounded by nine iron atoms; in the *Pnma*-II structure, by eight. The coordination polyhedron is a tricapped trigonal prism in the first case and a bicapped trigonal prism in the second. Phonon dispersion curves indicate the dynamic stability of both *Pnma* structures (Fig. 5).

Static calculations of the pressure dependence of enthalpy showed that the *Pnma*-I phase transforms into *Pnma*-II at 350 GPa (Fig. 6). The consideration of zero vibrations reduces the transition pressure to 315 GPa.

The calculation of the Gibbs energy suggests that *Pnma*-I is a low-temperature phase, which transforms into *Pnma*-II on heating to 600 K (Fig. 7). Thus, the *Pnma*-II phase is more favorable over the entire range of the Earth's core and mantle pressures and temperatures.

Search for structural analogs. The performed topological analysis showed that two carbides, Fe_3C-*I*-4 and Fe_2C-*Pnma*-I, belong to widespread structural types. The third structure, Fe_2C-*Pnma*-II, is described by new topology, which has no analogs in the structural database of inorganic compounds. For Fe_3C-*I*-4, 40 topological analogs were detected; for Fe_2C-*Pnma*-I, 406.

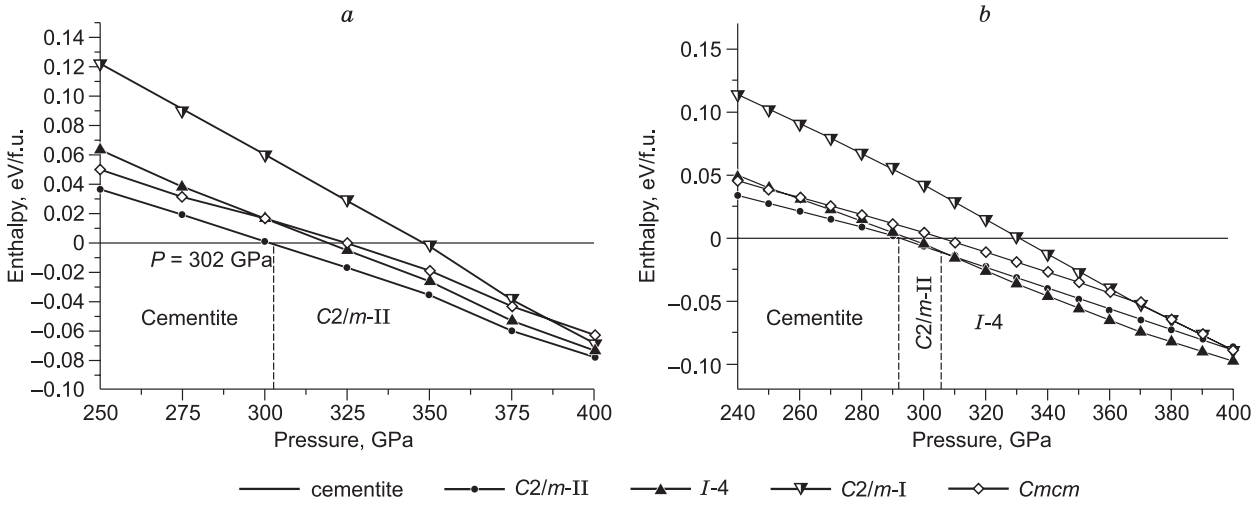

Fig. 2. Pressure dependence of enthalpy for Fe_3C without regard to vibrations (*a*) and with regard to zero vibrations (*b*) (*T* = 0 K).

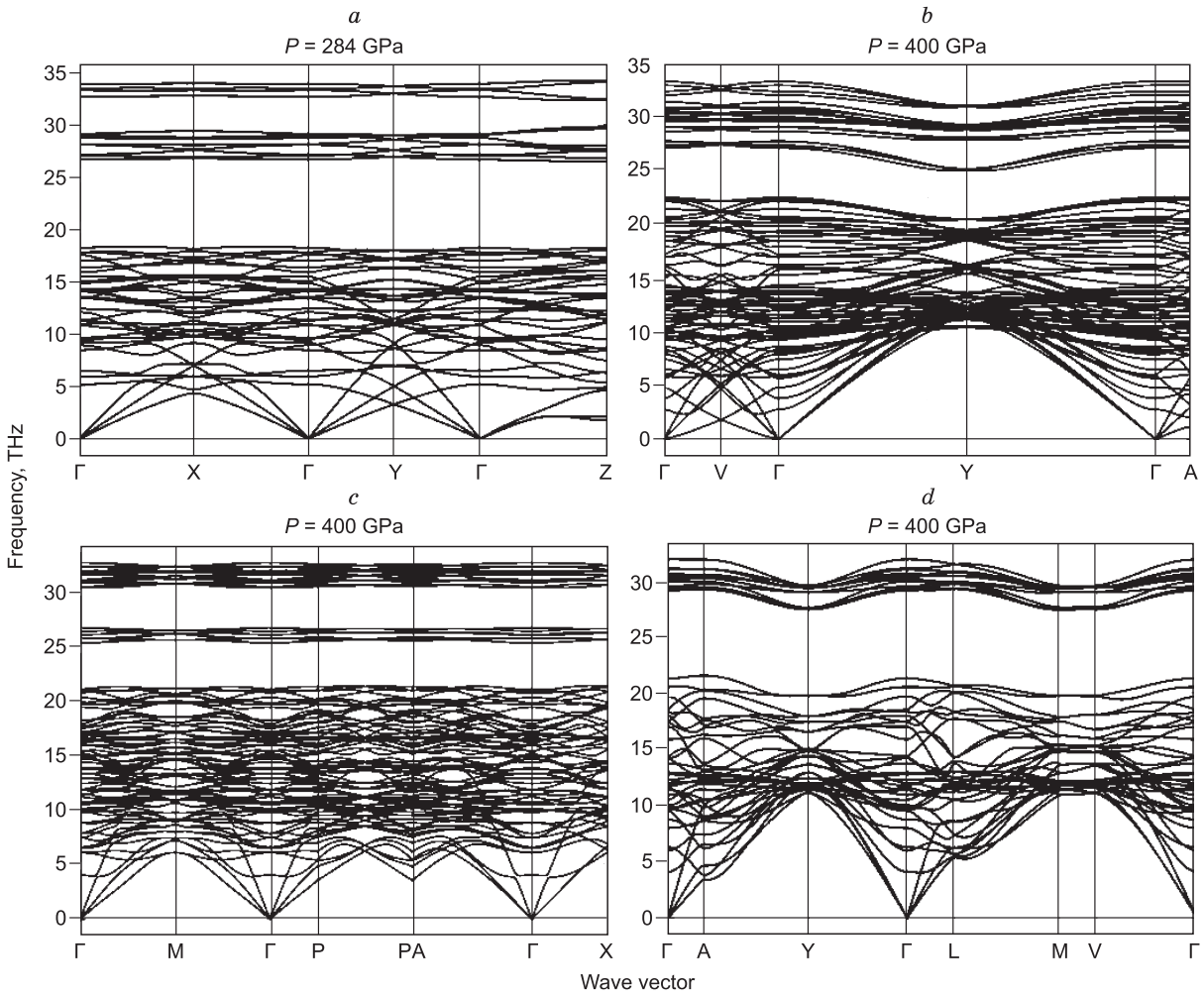

Fig. 3. Phonon dispersion curves of Fe_3C modifications: cementite (*a*), *C*2/*m*-I (*b*), *I*-4 (*c*), and *C*2/*m*-II (*d*).

Of 40 analogs of the Fe_3C-*I*-4 structure, there are 38 binary and two ternary compounds. Ten of 38 binary compounds belong to intermetallics. The chemically closest analogs are Fe_3P (Blanc et al., 1967), Fe_3S (Fei et al., 2000), and Fe_3B (Wang et al., 1980), as well as phosphides of transition metals: Ni_3P (Aronsson, 1955), Mn_3P (Spriggs, 1970), Nb_3P (Lomnitskaya et al., 1988), and Tc_3P (Rühl et al., 1982).

Of 406 analogs of Fe_2C-*Pnma*-I, 46 compounds are binary; 358 are ternary; one is quaternary; and 208 are intermetallics. The compounds Fe_2C-*Pnma*-I and Fe_2S-*Pnma* are structural analogs (Bazhanova et al., 2017). Despite the slight structural differences resulting in different topologies, these structures are very similar and can be regarded as structural analogs. Also, analogs were found among phosphides of transition metals—Co_2P (Rundqvist, 1960a) and Ru_2P (Rundqvist, 1960b).

Possible reactions of decomposition of iron carbides. Ab initio calculations indicate that Fe_7C_3 is unstable at pressures above 330 GPa and decomposes as follows: $Fe_7C_3 \rightarrow Fe_3C + 2Fe_2C$ (Weerasinghe et al., 2011). The possibility of this reaction at high temperatures is estimated below. The most favorable phase at the Earth's core pressure, h-Fe_7C_3, was chosen as a structure of Fe_7C_3 (Weerasinghe et al., 2011; Bazhanova et al., 2012; Raza et al., 2015). Based

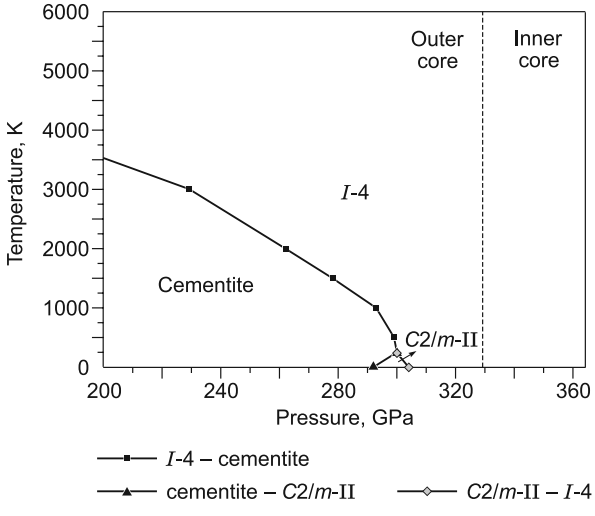

Fig. 4. *P*–*T* diagram for Fe_3C.

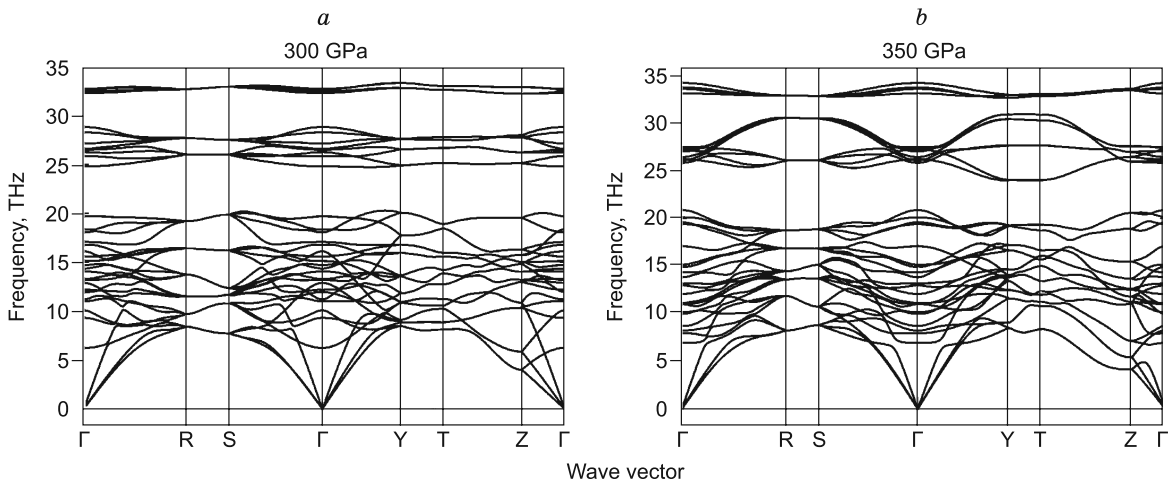

Fig. 5. Phonon dispersion curves of Fe_2C-*Pnma*-I (*a*) and Fe_2C-*Pnma*-II (*b*).

on the above calculation results, we chose the most favorable structures for Fe_3C and Fe_2C in the corresponding pressure intervals.

At 0 K, the decomposition of h-Fe_7C_3 becomes energetically favorable starting from 256 GPa (Fig. 8). On the *P–T* diagram, the boundary of this reaction has a curved shape with several kinks (Fig. 8*a*) caused by phase transitions in the reaction products Fe_3C and Fe_2C, which were described above. According to the *P–T* diagram, the mixture Fe_3C + Fe_2C is more energetically favorable than h-Fe_7C_3 over the entire range of the Earth's core pressures and temperatures. In this case the reaction products are stabilized owing to the transition of cementite into the *I*-4 phase (Fig. 8*b*).

Also, as a result of the transition of cementite into the *I*-4 phase, Fe_3C is stable with respect to the mechanical mixture Fe + Fe_2C over the entire range of pressures and temperatures. At a pressure of 329 GPa, which corresponds to the boundary between inner and outer cores, and a temperature of 0 K, the energy difference between Fe + Fe_2C and Fe_3C is 53.7 meV/f.u., and it increases as temperature increases. The trend of stability of iron carbides with respect to decomposition vs. pressure and temperature is seen on the convex hull (Fig. 9). The plotted convex hull suggests that

– at 100 and 200 GPa, Fe_3C and Fe_7C_3 are stable, which is consistent with the latest experimental data (Mashino et al., 2019);

– above 200 GPa, Fe_2C becomes stable, thus destabilizing Fe_7C_3 with respect to decomposition into Fe_3C + $2Fe_2C$;

– Fe_3C is stable over the entire range of pressures and temperatures.

For the Fe_3C-*I*-4 and Fe_2C-*Pnma*-II phases, which are stable at the pressures and temperatures of the inner core, density was calculated at 240–360 GPa, and it was compared with the density of the Earth's inner core.

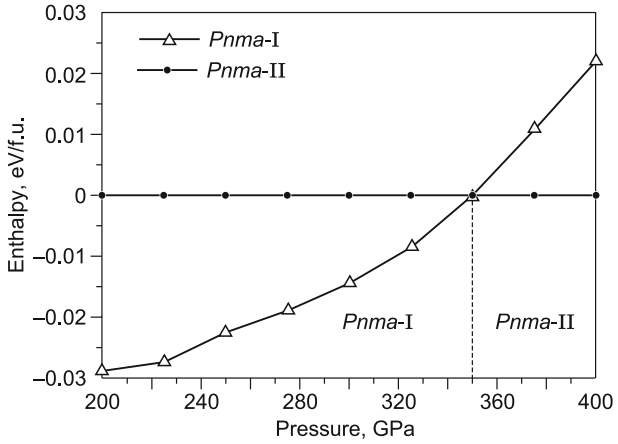

Fig. 6. Pressure dependence of enthalpy for *Pnma* modifications of Fe_2C.

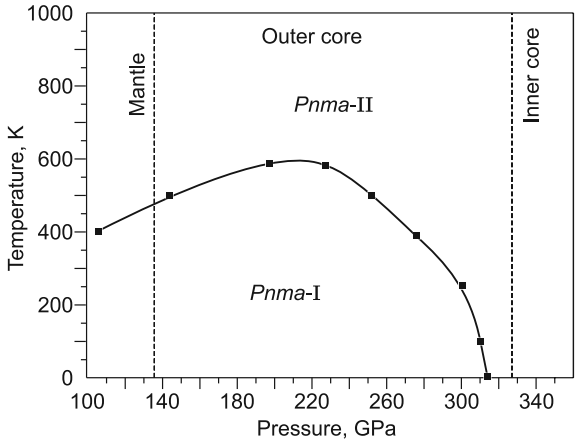

Fig. 7. Phase *P–T* diagram for Fe_2C.

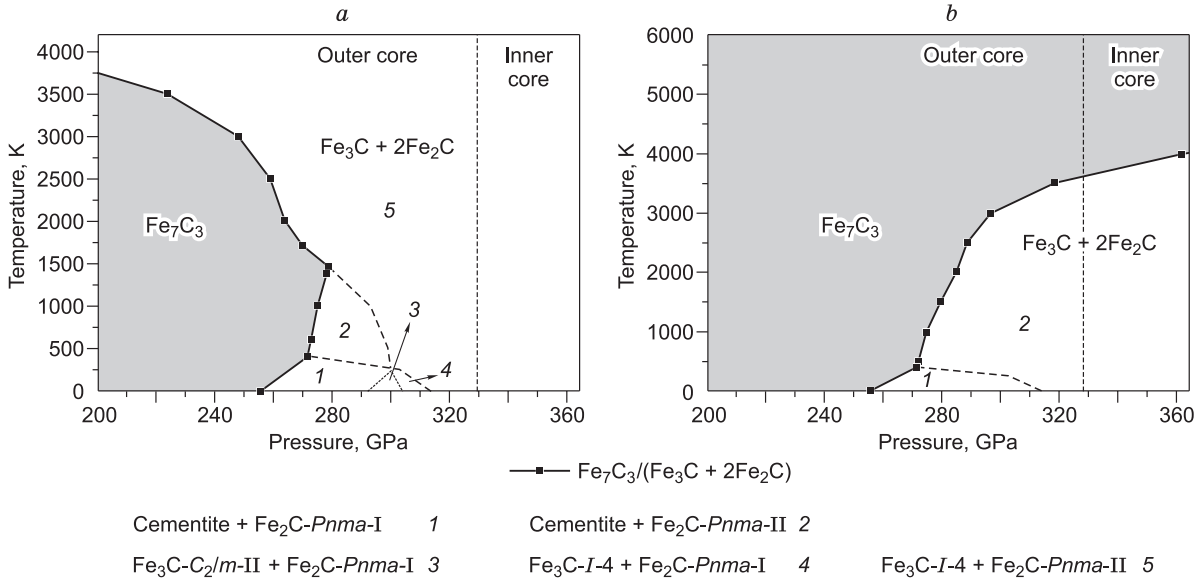

Fig. 8. Boundary of the $Fe_7C_3 \rightarrow Fe_3C + 2Fe_2C$ reaction on the *P–T* coordinates. Figures show the stability fields of the mixture $Fe_3C + 2Fe_2C$ for different combinations of Fe_3C and Fe_2C structures: *a*, With regard to all the stable phases of Fe_3C; *b*, with regard only to the cementite phase.

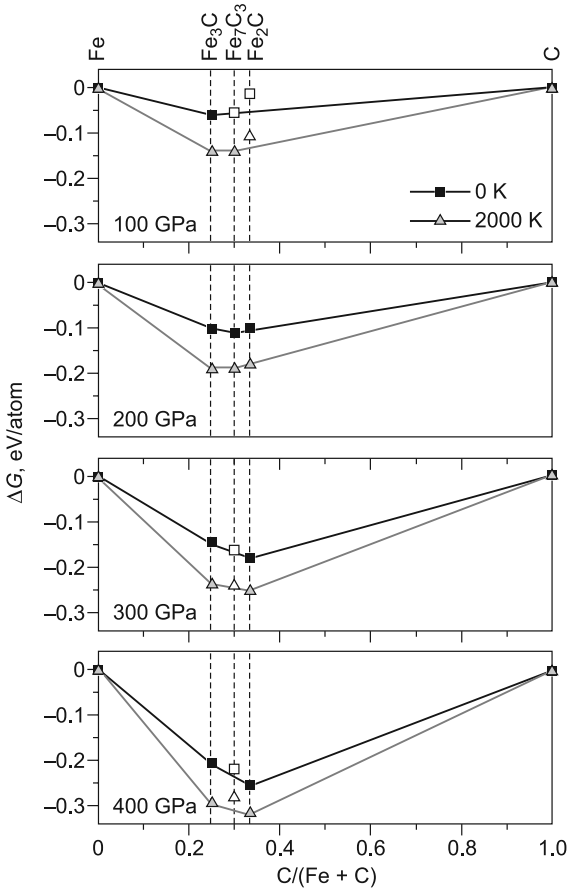

Fig. 9. Thermodynamic convex hull of the Fe–C system at 0 and 2000 K. Stable structures are marked by filled symbols; metastable structures, by blank symbols.

According to PREM (Dziewonski and Anderson, 1981), the density of the inner core is lower than that of hcp-Fe by 4.6–5.0% (Litasov and Shatskiy, 2016). The densities of the Fe_3C-*I*-4 and Fe_2C-*Pnma*-II phases were lower than the density of hcp-Fe by 8 and 12%. Thus, the density deficiency of the inner core with respect to hcp-Fe can be compensated for by extra 35.8–51.2 wt.% Fe_3C-*I*-4 at 5000–6000 K or by 23.1–33.4 wt.% Fe_2C-*Pnma*-II. Such carbide contents correspond to 2.4–3.5 wt.% C for the Fe_3C-*I*-4 phase and 1.5–2.3 wt.% for the Fe_2C-*Pnma*-II phase (Fig. 10; Table 3). The results presented in this paper are close to the estimates

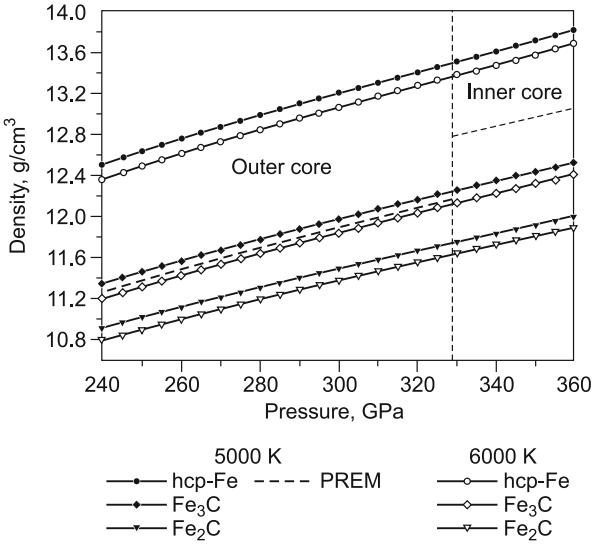

Fig. 10. Change in the densities of Fe_3C-*I*-4 and Fe_2C-*Pnma*-II at the Earth's core pressures and temperatures compared to PREM and pure hcp iron.

Table 3. Density of Fe_3C-*I*-4 and Fe_2C-*Pnma*-II compared to PREM and pure hcp iron

Phase	Temperature, K	ρ_{329GPa}, g/cm^3	ρ_{364GPa}, g/cm^3	C, wt.%	$\overline{M}$, a.m.u.
PREM		12.76	13.09		49
Fe_3C-*I*-4	5000	12.252	12.559	3.4–3.5	49.6
	6000	12.132	12.456	2.4–2.6	51.12
Fe_2C-*Pnma*-II	5000	11.742	12.03	2.2–2.3	51.63
	6000	11.638	11.928	1.5–1.7	52.7
hcp-Fe	5000	13.34	13.72		55.85
	6000	13.14	13.53		

based on calculations of Fe_2C density at 0 K: 2.6–3.7 wt.% (Bazhanova et al., 2012).

The cluster resources were kindly provided by the Computational Center of Novosibirsk State University.

The study was supported by the Russian Science Foundation, grant No. 17-17-01177.

REFERENCES

Aronsson, B., 1955. The crystal structure of Ni_3P. (Fe_3P-Type). Acta Chem. Scand. 9, 137–140.

Bazhanova, Z.G., Oganov, A.R., Gianola, O., 2012. Fe–C and Fe–H systems at pressures of the Earth's inner core. Phys. Usp. 55, 489–497.

Bazhanova, Z.G., Roizen, V.V., Oganov, A.R., 2017. High-pressure behavior of the Fe–S sytem and composition of the Earth's inner core. Phys. Usp. 60, 1025–1032.

Blanc, A., Fruchart, E., Fruchart, R., 1967. Etude magnetique et cristallographique des solutions solides $(Fe_{1-x}Cr_x)_3P$ et de la phase ferromagnetique Fe_5B_2P. Ann. Chim. 2, 251–254.

Blatov, V.A., 2006. Multipurpose crystallochemical analysis with the program package TOPOS. IUCr CompComm Newsl. 7 (4), 4–38.

Blatov, V.A., Shevchenko, A.P., Proserpio, D.M., 2014. Applied topological analysis of crystal structures with the program package ToposPro. Cryst. Growth Des. 14 (7), 3576–3586.

Chabot, N.L., Campbell, A.J., McDonough, W.F., Draper, D.S., Agee, C.B., Humayun, M., Watson, H.C., Cottrell, E., Saslow, S.A., 2008. The Fe–C system at 5 GPa and implications for Earth's core. Geochim. Cosmochim. Acta. 72 (16), 4146–4158.

Chen, B., Gao, L., Lavina, B., Dera, P., Alp, E.E., Zhao, J., Li, J., 2012. Magneto-elastic coupling in compressed Fe_7C_3 supports carbon in Earth's inner core. Geophys. Res. Lett. 39, L18301.

Dziewonski, A.M., Anderson, D.L., 1981. Preliminary reference Earth model. Phys. Earth Planet. Inter. 25 (4), 297–356.

Fei, Y., Li, J., Bertka, C.M., Prewitt, C.T., 2000. Structure type and bulk modulus of Fe_3S, a new iron-sulfur compound. Am. Mineral. 85 (11), 1830–1833.

Gavryushkin, P.N., Martirosyan, N.S., Inerbaev, T.M., Popov, Z.I., Rashchenko, S.V., Likhacheva, A.Y., Lobanov, S.S., Goncharov, A.F., Prakapenka, V.B., Litasov, K.D., 2017. Aragonite-II and $CaCO_3$-VII: new high-pressure, high-temperature polymorphs of $CaCO_3$. Cryst. Growth Des. 17 (12), 6291–6296.

Gavryushkin, P.N., Sagatov, N., Popov, Z.I., Bekhtenova, A., Inerbaev, T.M., Litasov, K.D., 2018. Structure and properties of new high-pressure phases of Fe_7N_3. JETP Lett. 107 (6), 379–383.

Glass, C.W., Oganov, A.R., Hansen, N., 2006. USPEX—Evolutionary crystal structure prediction. Comput. Phys. Commun. 175 (11–12), 713–720.

Hirotsu, Y., Nagakura, S., 1972. Crystal structure and morphology of the carbide precipitated from martensitic high carbon steel during the first stage of tempering. Acta Metall. Mater. 20 (4), 645–655.

Jack, K., 1951. Structural transformations in the tempering of high-carbon martensitic steels. J. Iron Steel Inst. 169, 26–36.

Kresse, G., Furthmüller, J., 1996. Efficiency of ab-initio total energy calculations for metals and semiconductors using a plane-wave basis set. Comput. Mater. Sci. 6 (1), 15–50.

Kresse, G., Joubert, D., 1999. From ultrasoft pseudopotentials to the projector augmented-wave method. Phys. Rev. B 59 (3), 1758–1775.

Kroumova, E., Aroyo, M.I., Pérez-Mato, J.M., Ivantchev, S., Igartua, J.M., Wondratschek, H., 2001. PSEUDO: a program for a pseudosymmetry search. J. Appl. Crystallogr. 34 (6), 783–784.

Litasov, K.D., Shatskiy, A.F., 2016. Composition of the Earth's core: A review. Russian Geology and Geophysics (Geologiya i Geofizika) 57 (1), 22–46 (31–62).

Litasov, K.D., Popov, Z.I., Gavryushkin, P.N., Ovchinnikov, S.G., Fedorov, A.S., 2015. First-principles calculations of the equations of state and relative stability of iron carbides at the Earth's core pressures. Russian Geology and Geophysics (Geologiya i Geofizika) 56 (1–2), 164–171 (214–223).

Lomnitskaya, Ya.F., Zakharets, L.I., Kondratyuk, G.D., 1988. Reaction of niobium and phosphorus with vanadium or chromium. Inorg. Mater. 24 (4), 610–614.

Lord, O.T., Walter, M.J., Dasgupta, R., Walker, D., Clark, S.M., 2009. Melting in the Fe–C system to 70 GPa. Earth Planet. Sci. Lett. 284 (1–2), 157–167.

Lv, Z.Q., Sun, S.H., Jiang, P., Wang, B.Z., Fu, W.T., 2008. First-principles study on the structural stability, electronic and magnetic properties of Fe_2C. Comput. Mater. Sci. 42 (4), 692–697.

Lyakhov, A.O., Oganov, A.R., Valle, M., 2010. How to predict very large and complex crystal structures. Comput. Phys. Commun. 181 (9), 1623–1632.

Lyakhov, A.O., Oganov, A.R., Stokes, H.T., Zhu, Q., 2013. New developments in evolutionary structure prediction algorithm USPEX. Comput. Phys. Commun. 184 (4), 1172–1182.

Mashino, I., Miozzi, F., Hirose, K., Morard, G., Sinmyo, R., 2019. Melting experiments on the Fe–C binary system up to 255 GPa: Constraints on the carbon content in the Earth's core. Earth Planet. Sci. Lett. 515, 135–144.

Methfessel, M., Paxton, A.T., 1989. High-precision sampling for Brillouin-zone integration in metals. Phys. Rev. B, 40, 3616.

Momma, K., Izumi, F., 2011. VESTA 3 for three-dimensional visualization of crystal, volumetric and morphology data. J. Appl. Crystallogr. 44 (6), 1272–1276.

Monkhorst, H.J., Pack, J.D., 1976. Special points for Brillouin-zone integrations. Phys. Rev. B, 13, 5188.

Mookherjee, M., 2011. Elasticity and anisotropy of Fe_3C at high pressures. Am. Mineral. 96 (10), 1530–1536.

Nakajima, Y., Takahashi, E., Suzuki, T., Funakoshi, K.-I., 2009. "Carbon in the core" revisited. Phys. Earth Planet. Inter. 174 (1–4), 202–211.

Oganov, A.R., Glass, C.W., 2006. Crystal structure prediction using ab initio evolutionary techniques: Principles and applications. J. Chem. Phys. 124 (24), 244704.

Oganov, A.R., Glass, C.W., Ono, S., 2006. High-pressure phases of $CaCO_3$: crystal structure prediction and experiment. Earth Planet. Sci. Lett. 241 (1–2), 95–103.

Ono, S., Mibe, K., 2010. Magnetic transition of iron carbide at high pressures. Phys. Earth Planet. Inter. 180 (1–2), 1–6.

Perdew, J.P., Burke, K., Ernzerhof, M., 1996. Generalized gradient approximation made simple. Phys. Rev. Lett. 77 (18), 3865–3868.

Pickard, C.J., Needs, R.J., 2006. High-pressure phases of silane. Phys. Rev. Lett. 97 (4), 045504.

Pickard, C.J., Needs, R.J., 2011. Ab initio random structure searching. J. Phys.: Condens. Matter 23 (5), 053201.

Raza, Z., Shulumba, N., Caffrey, N.M., Dubrovinsky, L., Abrikosov, I.A., 2015. First-principles calculations of properties of orthorhombic iron carbide Fe_7C_3 at the Earth's core conditions. Phys. Rev. B, 91 (21), 214112.

Rühl, R., Jeitschko, W., Schwochau, K., 1982. Preparation and crystal structures of technetium phosphides. J. Solid State Chem. 44 (1), 134–140.

Rundqvist, S., 1960a. Phosphides of the platinum metals. Nature 185, 31–32.

Rundqvist, S., 1960b. The structures of Co_2P, Ru_2P and related phases. Acta Chem. Scan. 14, 1961–1979.

Sata, N., Hirose, K., Shen, G., Nakajima, Y., Ohishi, Y., Hirao, N., 2010. Compression of FeSi, Fe_3C, $Fe_{0.95}O$, and FeS under the core pressures and implication for light element in the Earth's core. J. Geophys. Res. 115, B09204.

Smith, D., Lawler, K.V., Martinez-Canales, M., Daykin, A.W., Fussell, Z., Smith, G.A., Childs, C., Smith, J.S., Pickard, C.J., Salamat, A., 2018. Postaragonite phases of $CaCO_3$ at lower mantle pressures. Phys. Rev. Mater. 2 (1), 013605.

Spriggs, P.H., 1970. An investigation of the variation of lattice parameters with composition along the tie-line Ni_3P-Fe_3P. Philos. Mag. 21 (173), 897–901.

Stokes, H.T., Hatch, D.M., 2005. FINDSYM: program for identifying the space-group symmetry of a crystal. J. Appl. Crystallogr. 38 (1), 237–238.

Takahashi, S., Ohtani, E., Sakai, T., Hirao, N., Ohishi, Y., 2012. AGU Fall Meeting Abstracts. AGU, San Francisco, MR11B-2489.

Togo, A., Tanaka, I., 2015. First principles phonon calculations in materials science. Scr. Mater. 108, 1–5.

Vočadlo, L., Brodholt, J., Dobson, D.P., Knight, K.S., Marshall, W.G., Price, G.D., Wood, I.G., 2002. The effect of ferromagnetism on the equation of state of Fe_3C studied by first-principles calculations. Earth Planet. Sci. Lett. 203 (1), 567–575.

Wang, W.-K., Iwasaki, H., Fukamichi, K., 1980. Effect of high pressure on the crystallization of an amorphous $Fe_{83}B_{17}$ alloy. J. Mater. Sci. 15 (11), 2701–2708.

Weerasinghe, G.L., Needs, R.J., Pickard, C.J., 2011. Computational searches for iron carbide in the Earth's inner core. Phys. Rev. B, 84 (17), 174110.

Weerasinghe, G.L., Pickard, C.J., Needs, R., 2015. Computational searches for iron oxides at high pressures. J. Phys.: Condens. Matter 27 (45), 455501.

Wood, B.J., 1993. Carbon in the core. Earth Planet. Sci. Lett. 117 (3–4), 593–607.

Wood, B.J., Li, J., Shahar, A., 2013. Carbon in the core: its influence on the properties of core and mantle. Rev. Mineral. Geochem. 75 (1), 231–250.

Editorial responsibility: Yu.N. Palyanov